

Low pressure conversion of CO₂ to methanol over Cu/Zn/Al catalysts. The effect of Mg, Ca and Sr as basic promoters

Previtali D.^a, Longhi M.^b, Galli F.^{c,*}, Di Michele A.^d, Manenti F.^a, Signoretto M.^e, Menegazzo F.^e, Pirola C.^b

^a*Dipartimento di Chimica, Materiali e Ingegneria Chimica "Giulio Natta", Politecnico di Milano, piazza Leonardo da Vinci 32, 20133 Milano, Italy*

^b*Dipartimento di Chimica, Università degli Studi di Milano, via Golgi 19, 20133, Milano, Italy*

^c*Department of Chemical Engineering, Polytechnique Montréal, C.P. 6079, Succ. CV Montréal, H3C 3A7, Québec, Canada*

^d*Dipartimento di Fisica e Geologia, Università degli Studi di Perugia, via Pascoli 1, 06123 Perugia, Italy*

^e*Dipartimento di Scienze Molecolari e Nanosistemi, Università Ca' Foscari Venezia, via Torino 155, 30170 Venezia Mestre, Italy*

Abstract

Carbon dioxide concentration level is reaching a non-returning point. Carbon capture technologies are immature and short-term actions are necessary. The conversion of CO₂ into methanol is a technical challenge. Commercial copper-zinc-alumina catalysts convert maximum 7% carbon dioxide in syngas at high pressures (5 MPa to 10 MPa) and moderate temperatures (473 K to 573 K) into methanol. However, there are not records on the synthesis of methanol at low pressure ($P < 2.5$ MPa) and without a large excess of hydrogen in the feed. Here, we tested three new catalysts prepared by co-precipitation of copper, zinc and aluminum nitrates (CZA), with strontium, magnesium or calcium as basic promoters to enhance CO₂ conversion to methanol. We discussed the microstructure of the catalysts according to the supersaturation of the relative carbonates formed during the co-precipitation synthesis. Compared to the benchmark, the sample doped with Ca showed higher carbon conversion with all the feed compositions tested (syngas, synthetic biosyngas and CO₂ with H₂). CZA doped with Sr is inactive in this reaction.

Keywords: Methanol, CZA, Ca doped CZA, CO₂, Low pressure

1. Introduction

2 In December 2015, at the Paris United Nations Framework Convention on Climate Change
(UNFCCC), 195 nations agreed to take action to stop global warming. The goal is to decrease the
4 average temperature 2K above the value at the pre-industrial level. This target is ambitious, yet
feasible [1]. There is 66% chance to reach the objective if CO₂ quantity in atmosphere reduces by
6 1000 Gt compared to 2011. Thanks to the exponential increase in wind and solar energy deployment
[2] green electricity will be available at a competitive cost, as it is not linked to oil prices [3], but
8 actions are necessary to block emissions now, as a short-term strategy.

*Corresponding author

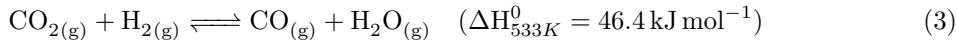
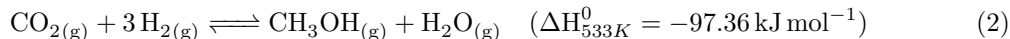
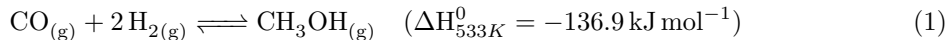
Email address: federico.galli@polymtl.ca (Galli F.)

The EPA estimates that most of the emissions of carbon dioxide derive from combustion to produce energy (fuel, electricity, etc.); 21 % of the total global greenhouse emissions account for the industrial sector [4]. Green energy sources (even though intermittent) are available (solar, wind, marine) while alternative carbon feedstock to produce chemicals lack.

In the period 2017-2020, 9839 scientific documents have been published regarding carbon dioxide capture and storage (CCS) (research made the 27/03/2020 in the *Topic* field of Web of Science Core Collection with the keywords “(carbon dioxide capture) OR (Carbon capture and storage)”). CCS technologies rely on the absorption and mineralization of carbon dioxide over solids or liquids [5]. However, high process costs [6] and technical issues, such as corrosion [7], limit the expansion of CCS at larger scale. Hansan et al. estimated that the sequestration of CO₂ whose concentration in a gas stream is higher than 10 % costs from 30 \$/t to 70 \$/t of CO₂, depending on the flow rate and the composition of the exhausted [8]. Moreover, a survey conducted in Germany in 2016 revealed that population rejects the CSS (sub-sea) compared to alternative remedies such as afforestation because of a general skepticism [9].

According to the IEA [10], CCS, CCSU, reduction of upstream oil consumption, nuclear energy and energy switching could decrease the CO₂ emissions up to 28 %. The impact on the total emissions of the production of fuels or chemicals from CO₂ could represent a reduction between 5 % to 20 % of them [11, 12, 13].

Converting CO₂ into chemicals or fuel is another profitable strategy that enables the reuse of carbon instead landfilling it. Methanol is a bulk chemical and a reagent for the production of various added value chemicals, like formaldehyde [14, 15], olefins [16, 17], biodiesel [18, 19, 20], aromatics [21, 22]. Methanol is an energy vector as well [23]. The annual world methanol production is increasing, in 2016 it was 80 Mt and it is expected to reach 100 Mt in 2020 [24]. The main reactions during the methanol synthesis are:



Methanol is produced by reaction 1 and 2, while reverse Water Gas Reaction (rWGS, reaction 3) consumes part of the hydrogen producing H₂O and CO. Methanol synthesis reactions are exothermic and catalyzed by copper and zinc (CZA catalyst), while rWGS is an endothermic reaction. The atomic molar ratio of a CZA (Cu/ZnO/Al₂O₃) commercial catalyst is 60/30/10 with 1 % to 3 % by weight of MgO. Cu and Zn oxide, with alumina as structural promoter, catalyze the hydrogenation of CO [25]. The catalyst activity depends on the copper exposed area [26]. Assuming a regular distribution of copper, zinc and dopants, the higher the surface area the greater the activity of the catalyst is [27]. MgO increases the catalyst lifetime, stabilizing the CZA structure and avoiding decreasing of the exposed copper area due to thermal sintering [28]. However, MgO inhibits methanol formation [28, 29]. In methanol synthesis reactions, the moles of products are lower than the moles of reactants (Eq.1 and 2), therefore high pressures thermodynamically favor methanol formation. Industrial reactors typically operate at a pressure from 5 MPa to 10 MPa [30, 31] with average CO conversion per pass of 25 % and a selectivity towards methanol over 99 % [32]. Moderate temperatures (473 K to 573 K) avoid thermodynamic limitations due to the reaction exothermicity. CO₂ is co-fed in low percentages (from 0.5 % to 5 %) to increase

42 methanol productivity [33]. Data are available on carbon dioxide conversion at medium pressure
(over 5 MPa) while literature is lacking of data under 2.5 MPa. Working at lower pressures allows
44 energy and cost savings, which leads to a greener and more remunerative processes. For example,
a plant that produces methanol from water electrolysis and biomass gasification consumes about
46 10 % of the energy in gas compression [34]. Another limitation is the large excess of hydrogen
employed in the feed: Meshkini et al. employed a mixture of CO₂ and syngas with 87.8 % of
48 hydrogen [35]. This decreases the economic competitiveness of the process proposed and limits
its scale up. They reported that Mn and Zr improve the methanol space time yield after 60 h
50 of operation (500 g kg⁻¹ h⁻¹ and 520 g kg⁻¹ h⁻¹, respectively compared to 490 g kg⁻¹ h⁻¹ for the
undoped catalyst). As far as we know, no one tested the effect of calcium oxide on the catalyst
52 activity of CZA at low pressure. The ideal feed has the lowest pressure and percentage of hydrogen
possible (the stoichiometric amount). Here we test four different CZA catalysts in the conversion of
54 syngas, a simulated biosyngas and a stream of CO₂ and H₂ into methanol. We study a commercial
CZA by Alfa Aesar (CZA-C) and three catalysts prepared i) without the addition of Mg (CZA-S)
56 and two doped with either ii) Ca (CZA-Ca) or iii) Sr (CZA-Sr). This paper is original because:
we study the methanol synthesis with different gas composition but without an excess of hydrogen,
58 aiming at developing a more economical process performing the reaction at low pressure and we
test the activity of CZA-Ca and CZA-Sr, which was never reported in literature before. We also
60 characterized a sample prepared with the same co-precipitation method employing Mg as promoter.

2. Experimental

62 2.1. Catalyst synthesis

CZA catalysts were synthesized with a co-precipitation method [36]. Distilled water dissolved
64 metal nitrates precursors (Cu(NO₃)₂, Zn(NO₃)₂, Al₂(NO₃)₃, Mg(NO₃)₂, Sr(NO₃)₂, and Ca(NO₃)₂,
purity 95 %, Sigma Aldrich) with a total concentration of 1.0 mol L⁻¹ and a metal molar ratio of 60-
66 30-10-1, respectively for Cu, Zn, Al and X, where X is Ca, Mg or Sr. We selected this percentage to
avoid excessive covering of the basic promoter and to have a comparable concentration comparable
68 to the one employed in literature [29, 35, 37]. We added the metal solution to 200 mL of distilled
water in a jacket reactor. A syringe pump controlled the metal solution flow, set to 5 mL min⁻¹.
70 A thermocouple and a pHmeter monitored the operating condition. The simultaneous addition of
a Na₂CO₃ solution (1.0 mol L⁻¹) maintained the pH to a value of (7.0 ± 0.2) A thermostatic bath
72 set the temperature of the reactor to 343 K. After the metal solution addition, the mixture aged
for 1 h at 343 K and pH = 7. A Buchner filtered the blue precipitate. It was washed with 150 mL
74 of deionized water and dried at 353 K for 15 h in an oven. A furnace calcined the powder at 573 K
under static air for 3 h (ramp of 15 K min⁻¹). A sieve meshed the resulting catalyst in the range
76 106 μm to 136 μm to avoid mass transfer limitations in the reaction.

2.2. Characterization

78 We characterized all synthesized samples before testing them. A Micromeritics Tristar II ap-
paratus (Tristar II 3020) measured the Brunauer-Emmett-Teller (BET) specific surface area from
80 N₂ adsorption/desorption isotherms at 77 K [38]. Barret-Joyner-Halenda (BJH) method applied to
the N₂ adsorption data evaluated porosity distribution [39]. We pre-treated the samples at 423 K
82 for 4 h under a N₂ flow to remove adsorbed water and contaminants. A LEO1525 Field emission
scanning electron microscope (SEM) imaged all the samples. A Bruker Quantax EDX instrument
84 equipped on the SEM mapped elements' distribution on catalysts' surface. X-ray photoelectron

spectra (XPS) were taken in an M-probe apparatus (Surface Science Instruments). The source was
 86 monochromatic Al $K\alpha$ radiation (1486.6 eV). A Philips PW3020 diffractometer (XRD) collected
 88 samples' diffractograms from 10° to 65° with a step of 0.04° (step time of 10 s). Temperature pro-
 90 grammed reduction (TPR) analyses measured the reduction temperature of Cu to metal [40]. 50 mg
 92 of samples reacted with 40 mL min^{-1} of 5% of H_2 (in Ar) ramping the temperature from 298 K
 to 1173 K at 10 K min^{-1} . A thermoconductivity detector (TCD) measured H_2 uptake. A Mettler
 Toledo TGA/DSC 3+ characterized CZA-S before and after the synthesis and estimated the amount
 of carbon coke remained on the catalyst after the reaction. TGA measured weight variation of the
 sample under an air flux, ramping the temperature from 313 K to 973 K at 5 K min^{-1} .

94 2.3. Bench scale plant

We charged $(1.00 \pm 0.01) \text{ g}$ of catalyst in a 6.35 mm diameter reactor (teactor length = 560 mm).
 A blank test assured that its internal surface is inactive. Two pieces of quartz wool held the catalyst
 in place, in a fixed bed configuration. Prior to the test, 20 NmL min^{-1} of H_2 reduced the catalyst
in situ at 573 K for 3 h. Then, four mass flow controllers flowed nitrogen (internal standard for
 chromatographic analyses), carbon monoxide, hydrogen and carbon dioxide into the reactor. A
 pressure controller back-regulated the pressure to a value of 2 MPa. An electrical furnace heated the
 reactor to the desired temperature. A k-type thermocouple measured the reaction temperature right
 above the catalytic bed. We profiled the isothermal zone of the reactor (Supporting Information,
 Fig. S1). Reactants flow from the top to the bottom of the reactor with a GHSV of 4030 h^{-1} . Before
 the pressure controller, a cold trap ($T = (265 \pm 1) \text{ K}$) condenses the reaction products (methanol
 and water). A micro-GC (Agilent 3000A, carrier: He), equipped with a PlotQ and a MOLSIEVE
 columns, samples the exiting gases every 1 h. It calculates the flow of CO that exits the reactor
 ($F_{\text{CO},out}$) using the flow and peak area of the internal standard (N_2 , eq 4) and, therefore, CO
 conversion (X_{CO} , 5) [41]. The micro-GC also detects methanol that is not condensed.

$$F_{\text{CO},out} = F_{\text{N}_2,in} * \frac{\text{Area}_{\text{CO}}}{\text{Area}_{\text{N}_2}} \quad (4)$$

$$X_{\text{CO}} = \frac{F_{\text{CO},in} - F_{\text{CO},out}}{F_{\text{CO},in}} * 100 \quad (5)$$

$$S = \frac{F_{\text{H}_2,in} - F_{\text{CO}_2,in}}{F_{\text{CO}_2,in} + F_{\text{CO},in}} \quad (6)$$

At the end of each test, a GC-FID Fision 8000, equipped with a Porapak column QS, determined
 96 the methanol concentration in the cold trap, using acetone (Sigma Aldrich, 99% purity) as internal
 standard. The oven temperature was 573 K, the carrier was He at a inlet pressure of 100 kPa.
 98 The attenuation and the range were 1 and 2 respectively. We tested CZA-C, -S, -Ca and -Sr
 catalysts with: a) syngas, with a H_2/CO molar ratio of 2, to simulate a stoichiometric amount of
 100 reactants produced by methane steam reforming [42, 43], which is also the typical feed composition
 for Fischer-Tropsch reactors [44, 45, 46], b) syngas containing 5.6% of CO_2 , which is similar to
 102 the composition obtained by steam-gasification of biomass-derived oil (carrier gas: N_2 and $T =$
 104 1073 K) [47] and a H_2 concentration of 72%. In this feed, H_2 concentration was set to have a S
 value of 2.4 (eq 6). S considers the extra amount of H_2 that CO_2 consumes in the rWGS [48]. A
 value $S = 2$ corresponds to the stoichiometric H_2 quantity. Nevertheless, in commercial processes
 106 a value higher than 2 is employed (2.2-2.4). Finally, catalysts were tested with a c) stoichiometric

108 mixture of CO_2 and H_2 (1:3), to study the direct conversion of carbon dioxide into methanol (Table
 110 1). The reactor operated between 513 K to 533 K as most of CZAs have a maximum conversion of
 CO_2 [29]. We set the pressure to 2 MPa because Saeidi et al. [49] reported from many catalysts for
 CO_2 conversion this operating pressure.

Table 1: Summary of the experiments for CZA-C, CZA-S, CZA-Ca and CZA-Sr

Test	Temperature, K	Flow rate set, NmL min^{-1}			
		CO	H_2	CO_2	N_2
1	513	10.4	33.7	2.6	5.0
2	533	10.4	33.7	2.6	5.0
3	513	-	31.3	10.4	5.0
4	533	-	31.3	10.4	5.0
5	513	15.6	31.1	-	5.0
6	533	15.6	31.1	-	5.0

3. Results and discussion

112 During TGA analysis, CZA-S loses weight in the ranges 373 K to 473 K (Figure 1, A), 523 K to
 114 673 K (Figure 1, B) and, 723 K to 873 K (Figure 1, C), in accordance with the data reported by Gines
 et al. [50, 51]. Firstly, crystallized water contained in hydroxycarbonates evaporates. The complete
 116 dehydroxylation occurs as the second peak and the decarbonation with the loss of strongly bonded
 CO_3^{2-} constitutes the third peak [51]. During sample preparation, at 573 K, hydroxycarbonates
 partially dehydroxylate and decompose [52, 53], therefore oxides may form in this second step.
 118 XRD analyses confirm this observation. For CZA-S, CZA-Ca and CZA-Mg, indeed, typical peaks
 of copper and zinc oxide are observed (Figure 2). Moreover, in CZA-Ca peaks of crystalline CaCO_3
 120 are also evidenced (Circular of the Bureau of Standards n. 539: standard X-ray diffraction powder
 patterns). CZA-Sr has a similar behavior, with the presence of SrCO_3 . In CZA-Mg, MgCO_3 peaks
 122 are absent (Figure 2), as also observed in [51], even though also its degradation temperature is
 higher than 573 K.

124 Mg^{2+} has a radius close to copper and the same charge [54] and therefore it substitutes copper in
 the lattice, without forming MgCO_3 , which is not detected in XRD spectra. CZA-S and CZA-C have
 126 a similar structural morphology, *i.e.* agglomerated spherical particles randomly organized (Figure 3a
 - 3d). Doping the catalyst with Ca and Sr induces the formation of well-organized rod-like structures
 128 constituted by smaller nanoparticles. Sr makes the rods cover the main structure (Figure 3g and
 3h). Baltes et al. obtained a similar conformation applying the same synthesis conditions [36].
 130 These structures are similar to polycrystalline calcite needle-fiber, formed by random precipitation
 around nuclei in the presence of highly supersaturated solution [55]. These columnar structures are
 132 absent in CZA-Mg (Figure 3i-3j), whose morphology is similar to CZA-S. These differences are due
 to carbonates water solubility (MgCO_3 , $1.4 \times 10^{-1} \text{ g L}^{-1}$, CaCO_3 , $1.4 \times 10^{-2} \text{ g L}^{-1}$, and SrCO_3 ,
 134 $3.4 \times 10^{-3} \text{ g L}^{-1}$ [56, 57]), that induces a different relative supersaturation (RS) of these salts in
 solution during the synthesis ($RS = 0, 11$ and 73 for MgCO_3 , CaCO_3 , SrCO_3 , respectively). Indeed,
 136 during the precipitation step, alongside the formation and growth of hydroxycarbonates (the core
 of CZA), alkaline earth metal carbonates form and are stable at the synthesis conditions [58, 50].
 138 In our synthesis, the concentration of MgCO_3 was not in supersaturated conditions.

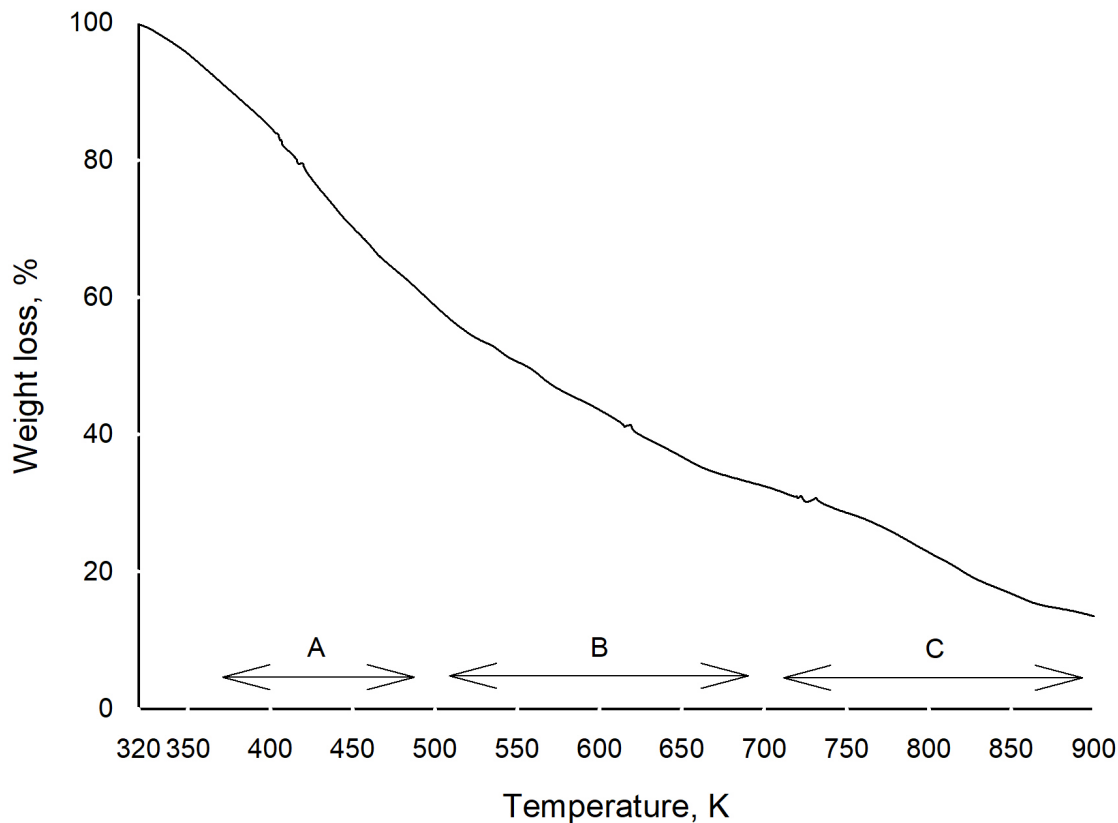


Figure 1: Thermal Gravimetric Analysis of CZA-S

Hydroxycarbonates have a $\text{pH}_{\text{p.z.c.}}$ above 7 [59]. The pH during the synthesis is about 7,
 140 and hydroxycarbonates, positively charged, attract negative species as carbonates that interact
 preferably with the formed solid rather than dissolved cations in solution [60]. These particles
 142 attract the solute clusters (embryos) by Van der Waals forces [61]. The concentration of embryos in
 the proximity of the forming crystals depends on the supersaturation of the solution, the larger the
 144 RS the higher their concentration [61]. When RS is large a rapid coagulation happens, leading to
 the formation of nuclei greater than a critical size, above which there is the nucleation [61]. These
 146 superstructures based on chaotically assembled nanoparticles precipitate on the hydroxycarbonates.
 This phenomenon is defined as secondary nucleation and is responsible of the structures observed
 148 when doping with Ca and Sr. The difference between these two alkaline earth metals is related to
 the different RS value, being in the case of Sr higher than Ca. In the case of doping with Mg, the
 150 solution is not supersaturated and these structures do not grow.

These structures affect the porosity distribution (Figure 4) in the range of pores between 2 nm
 152 to 10 nm. In fact, doping with Ca and Sr, the amount of pores in this range is higher than in the

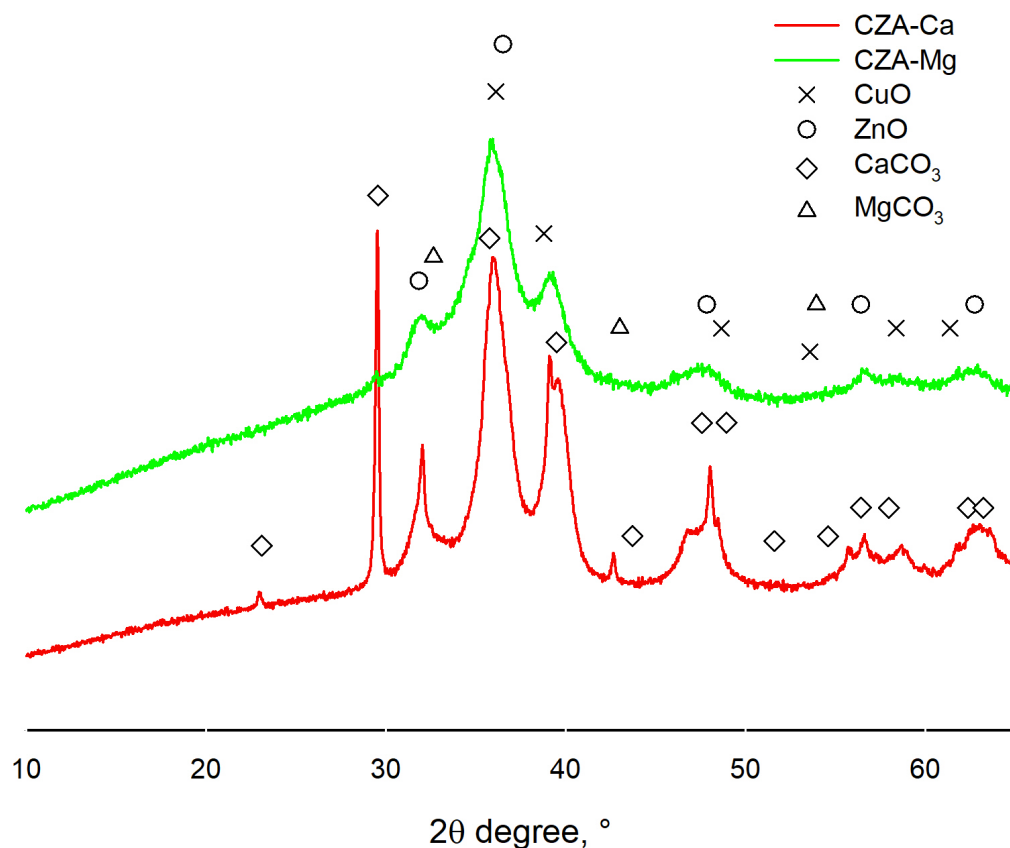


Figure 2: XRD analyses

154 case of both CZA-S and CZA-C. This difference is due to the porosity created between the building-
 blocks of the rod-like structures. The growth of these structures may also explain the lower specific
 156 surface area and pore volumes of these materials (Table 2) compared to commercial and undoped
 samples. In fact, the secondary nucleation, responsible of these structures, may take place both
 158 onto the surface and in bigger pores, partially occluding them and provoking a decrease of both
 specific surface area and pore volume. Indeed, samples without rod-like structures possess similar
 specific surface area. Moreover, CZA-C does not present micropores, while all the other samples
 160 do. The majority of pores diameters' fall in the range 2 nm to 10 nm (above 40 %), especially in
 the case of commercial sample (90 % of the total). However, in CZA-Ca e CZA-Sr these pores are
 162 in a lower amount than in the other samples, and this might be justified considering the formation
 of rod-like structures as stated above.

164 All catalysts start to reduce in the range 473 K to 493 K, with a sharp peak from 539 K to 557 K,
 which corresponds to the transformation of CuO into Cu⁰ (Figure 5), in accordance with literature

166 [62, 63]. Therefore, the activation temperature chosen permitted to reduce copper. All samples
168 present a minor and broad reduction peak between 873 K to 1043 K. It corresponds to the partial
170 reduction of ZnO [64]. TPR confirms the presence of a sole copper species for CZA-S at 573 K,
172 ascribable to the reduction of highly dispersed CuO [65]. The peak position of CZA-Mg is similar
to that of CZA-S, with a broad peak between 593 K to 653 K. Ca and Sr doping shifts and broadens
the reduction peak of CZA (inset of Figure 5) because of the stronger interaction between the two
lattice of CuO and ZnO [66].

SEM-EDX analysis shows a good distribution of each metals for all catalyst samples (see Sup-
174 porting Information, Figure S2-S4) and no traces of carbon (coke) were present on the spent cata-
lysts. TGA diagrams report an increase of weight for CZA-S. This phenomenon is probably caused
176 by copper oxidation. When CZA is discharged, the reactor is cold ($T = 303$ K) and not all the
metallic copper is oxidized by atmospheric oxygen. The remaining Cu^0 reacts during the TGA
178 analysis and CuO formation determines an increase in weight. This theory is confirmed also by the
fact that the weight gain usually is 1.3 mg which corresponds to the quantity of oxygen necessary
180 to oxidizes about 10 % of the all metallic copper (see Supporting Information, Figure S5). XPS
reports a surface enrichment of aluminum, as also reported in [67]. Its concentration reaches the
182 maximum in the first layers of the particles (XPS measures from 38 % to 40 % atomic percentage
of Al) and decreases after few micrometers depth (SEM-EDX measures from 7 % to 8 % atomic
184 percentage of Al). This enrichment is due to the hydrolysis of the nitrate system [68].

All the catalytic tests have a mass balance for carbon and oxygen over 90 %. With syngas
186 (CO/H_2) as feed, the carbon conversion is higher at 533 K (Figure 6b) due to kinetic reasons.
We did not observe the typical volcano-shape curve for CO conversion because we operated the
188 reactor at only two temperatures, near to the average maximum value (523 K, [29]) to have a
comparison of the catalysts at similar thermodynamic and kinetic conditions. The activity of CZA-
190 Ca is significantly higher (12 % CO conversion (Tab 3) respect to 9 % for CZA-S) already at 513 K
and increases at 533 K producing more than the double amount of products respect to CZA-C
192 and maintaining a similar methanol content in the condensed fraction (Figure 7). CZA-S has an
overall productivity similar to CZA-Ca at 513 K but with a methanol concentration lower than
194 20 % (Figure 7) by weight. The presence of Ca and Mg (the latter contained in CZA-C) limits
the rWGS, the main source of water, at 513 K and 533 K where its endothermicity favors water
196 formation. At 513 K, CZA-Ca has a stationary CO conversion value of about 5.6 % while CZA-S
the one with the lower conversion (3.9 %). At 533 K the same trend was observed (11.5 % versus
198 9.1 %, Tab 3). This is confirmed by the productivities of both methanol and water (Figure 7).
With syngas, Ca improves methanol formation by 3 times while the water content remains low
200 (about 30 % by weight). CZA-S has the worst performances as methanol productivity and as water
content. The pore size dimension and distribution does not have an effect on CO or CO_2 conversion
202 and methanol productivity.

With CO_2/H_2 as feeding mixture, temperature has a negligible influence on CO_2 conversion
204 with CZA-C. The same trend is obtained observing the productivities (Figure 7). Due to the large
presence of CO_2 and H_2 , high temperature favors the reverse Water Gas Shift reaction (rWGS)
206 increasing the water and CO productivity while methanol concentration in the liquid product
decreases. For this reason, with this feed are obtained the highest values of water concentration.
208 CZA-C is the more stable varying the temperature while both CZA-Ca and CZA-S show an increase
in CO_2 conversion of 2 or 3 times. Also in this case an increase of temperature cause a decreasing
210 of methanol concentration. CZA-Sr resulted the least active.

Using as feed the mixture of CO and CO_2 at 513 K, the more active catalyst is CZA-S followed

Table 2: BET area, pore volume and surface composition results (EDX and XPS) for all catalysts synthesized

Catalyst	Morphology		Chemical composition						
	BET area $\text{m}^2 \text{g}^{-1}$	Pore volume $\text{m}^3 \text{g}^{-1}$	Al	Cu	Zn atomic %, XPS / EDX (± 0.5)	O XPS / EDX (± 0.5)	Mg	Ca	Sr
CZA-C	100 ± 1	0.19	40.2 / 7.8	12.8 / 21.2	8.8 / 9.6	38.2 / 60.4	- / 1.5	-	-
CZA-S	94.9 ± 0.4	0.49	34.6 / 8.1	13.0 / 15.5	10.0 / 10.1	42.4 / 66.4	-	-	-
CZA-Ca	81.8 ± 0.4	0.28	38.6 / 8.3	11.6 / 17.7	7.0 / 13.8	42.8 / 60.0	-	0.0 / 0.2	-
CZA-Sr	71.8 ± 0.3	0.28	44.0 / 6.8	12.2 / 33.3	6.1 / 15.0	37.7 / 44.1	-	-	0.0 / 0.7
CZA-Mg	97.1 ± 0.3	0.59	32.8 / 1.1	3.8 / 29.4	5.1 / 8.5	33.3 / 61.0	25.0 / 0.1	-	-

212 by CZA-C (about 20 % less, Tab 3) and CZA-Ca with the lowest productivity For CZA-C at 533 K
 214 the productivity increases despite the CO conversion decreases. This could be explained by an
 increase of selectivity of CO₂ to methanol instead of to CO and water (rWGS). This effect is
 216 emphasized with CZA-S where no promoters are present. Liu et al. obtained the same result with
 a Cu based catalyst supported on titania and modified with 1 % of MgO [69]. They explained this
 218 behavior considering kinetics and thermodynamics. The presence of MgCO₃ results in a stronger
 CO₂ adsorption that improves its activity in terms of conversion. CaCO₃ is a stronger base than
 MgCO₃, and indeed the CO₂ conversion increases (Figure 6). CZA-C and CZA-Ca maintain similar
 220 productivity in terms of liquid quantity and composition at the two temperature tested. However,
 for CZA-S, increasing the temperature, the methanol formation is halved. CZA-Ca has the lowest
 222 productivities at both temperatures among the active catalysts, while CZA-Sr resulted inactive
 with this feed (CO conversion lower than 3 % for both the temperatures tested). Phongamwong
 224 et al. [70] derived an equation to calculate methanol selectivity and to assess the quantity of
 CO₂ converted to methanol (Table 4). Except for CZA-Sr, which resulted inactive for the negligible
 226 amount of methanol condensed in the cold trap, all the catalysts increases CO₂ conversion into
 CH₃OH at 533 K. Therefore, higher temperature activates carbon dioxide for this reaction. CZA-S
 228 and CZA-Ca resulted superior, probably because of the larger pore volume available compared to
 CZA-C (Table 2). The stationary state conversion of carbon at 513 K and 533 K demonstrated
 230 that the best promoter is not the most basic (Figure 6), indeed Ca resulted the most active sample
 for all the feedstock tested. A deeper investigation on the diverse carbonate stability at different
 232 temperature and CO₂ partial pressures and on the dimension of the crystallites may correlate these
 findings.

234 Our materials are better than commercial one, and among home-made catalysts CZA-Ca shows
 with CO/H₂ and CO₂/H₂ the best performance in terms of methanol yield. These results may
 236 be justified considering porosity results. Despite many factors influence methanol yield, as stated
 by Li et al. [71], specific surface area has a great effect in this process, but pore volume and
 238 mesoporosity centered between 2 nm to 10 nm are both more pivotal. CZA-C possesses the highest
 specific surface area but also the lowest pore volume (Table 2), even if pores are centered in the
 240 optimal range, whilst CZA-Ca is characterized by a lower specific surface area and amount of pores
 centered in small mesopores but a larger pore volume (Table 2). For the other samples the results
 242 can be justified considering the combination between pore volume and mesoporosity. These data
 show that porosity and its distribution are important for catalytic activity in this process.

Table 3: Carbon conversion and sample standard deviation (in parenthesis) for all the tests.

Temperature, K	513			533			
	Feed	H ₂ /CO	H ₂ /CO/CO ₂	H ₂ /CO ₂	H ₂ /CO	H ₂ /CO/CO ₂	H ₂ /CO ₂
	CZA-S	4.0(0.2)	31.9(0.4)	16.0(0.5)	9.0(0.1)	23.4(0.2)	19.4(0.4)
	CZA-C	5.4(0.1)	27.5(0.2)	19.0(1.0)	10.3(0.1)	20.3(0.3)	20.8(0.5)
	CZA-Ca	5.7(0.1)	29.6(0.4)	20.3(0.8)	11.5(0.1)	21.8(0.4)	22.5(0.4)
	CZA-Sr	2.7(0.1)	3.2(0.1)	9.2(0.3)	5.5(0.1)	3.0(0.1)	14.2(0.2)

Table 4: Methanol selectivities and fraction of CO₂ converted into CH₃OH for the tests with CO₂ and syngas co-fed [70]. Uncertainties are reported in parenthesis with a confidence interval of 95 %

Temperature, K	CH ₃ OH selectivity, %		CO ₂ to CH ₃ OH, %	
	513	533	513	533
CZA-C	0.2(0.0)	0.1(0.0)	3.8(0.1)	5.7(0.1)
CZA-S	0.4(0.0)	0.5(0.0)	4.3(0.3)	7.3(0.2)
CZA-Ca	0.2(0.0)	0.3 (0.0)	4.2(0.2)	6.5(0.2)
CZA-Sr	0.0 (-)	0.0 (-)	0.0(-)	0.0(-)

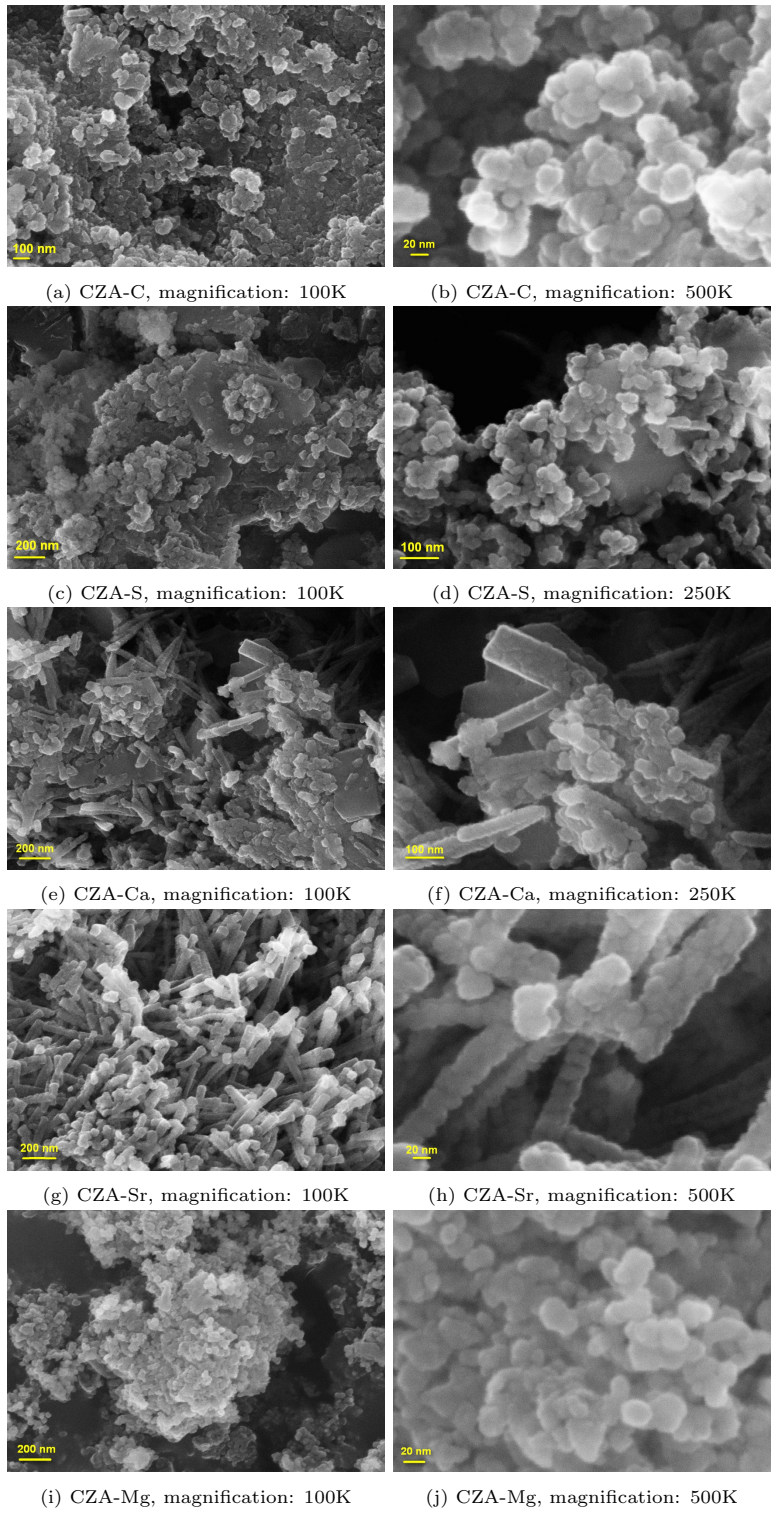


Figure 3: SEM images of commercial and synthesized CZA

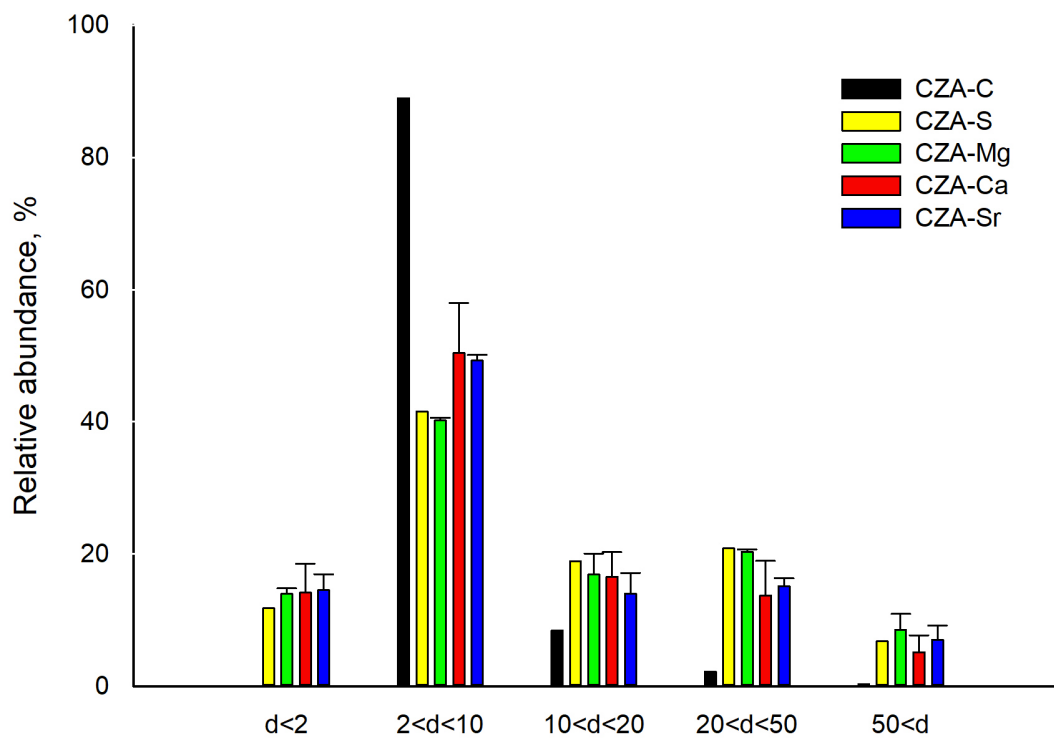


Figure 4: Pore diameter distribution obtained from BJH model (adsorption branch of the isotherm)

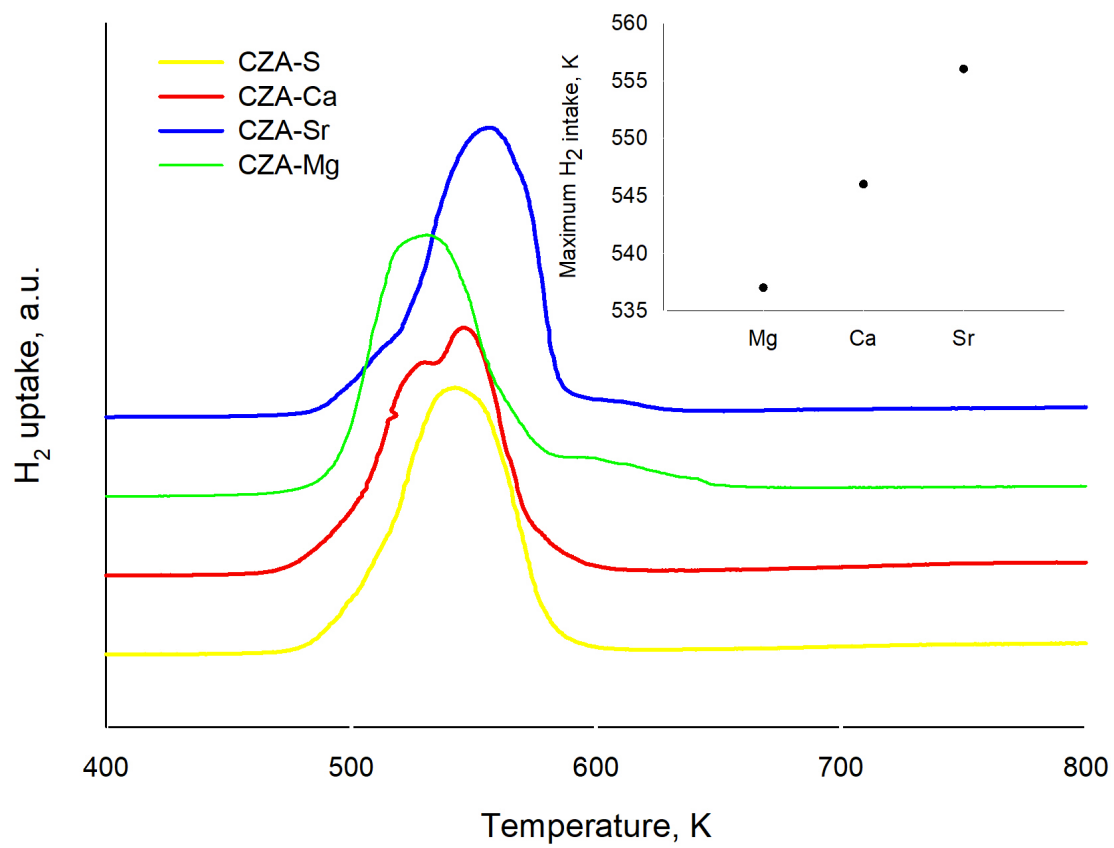


Figure 5: Temperature programmed reduction of the synthesized catalysts

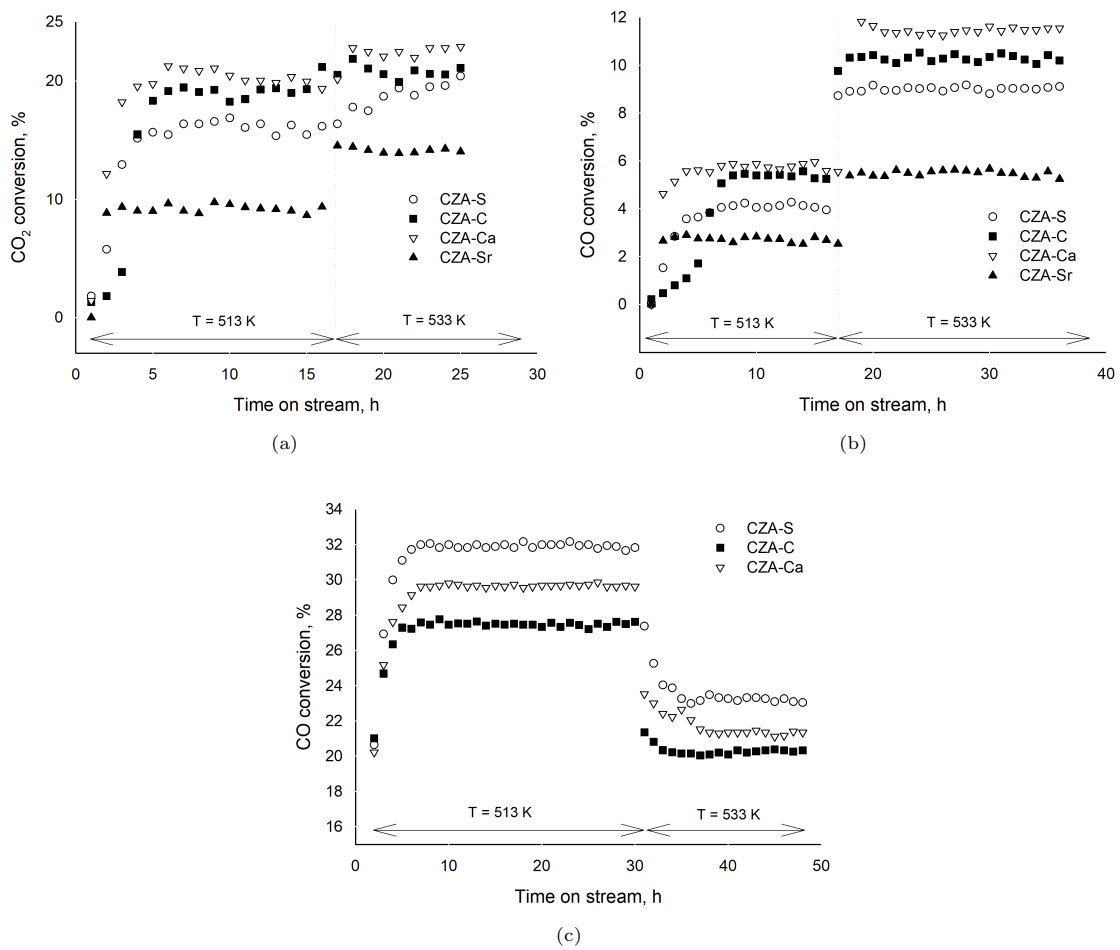


Figure 6: Conversion of CO₂ or CO for all catalysts with different feed compositions: CO₂ and H₂ (a), CO and H₂ (b) and CO₂, CO and H₂, (c). CZA-Sr resulted inactive with this latter stream.

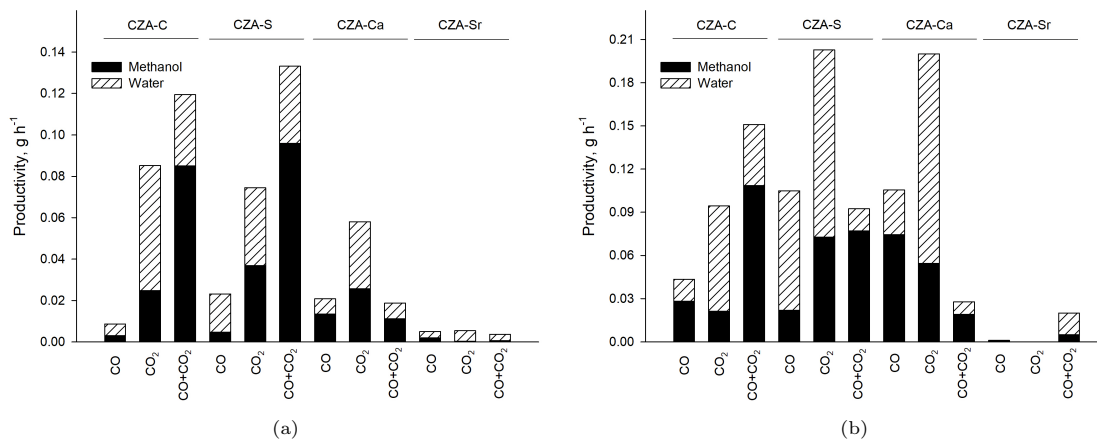


Figure 7: Methanol and water productivity (divided by the total test time) at 513 K (a) and 533 K (b)

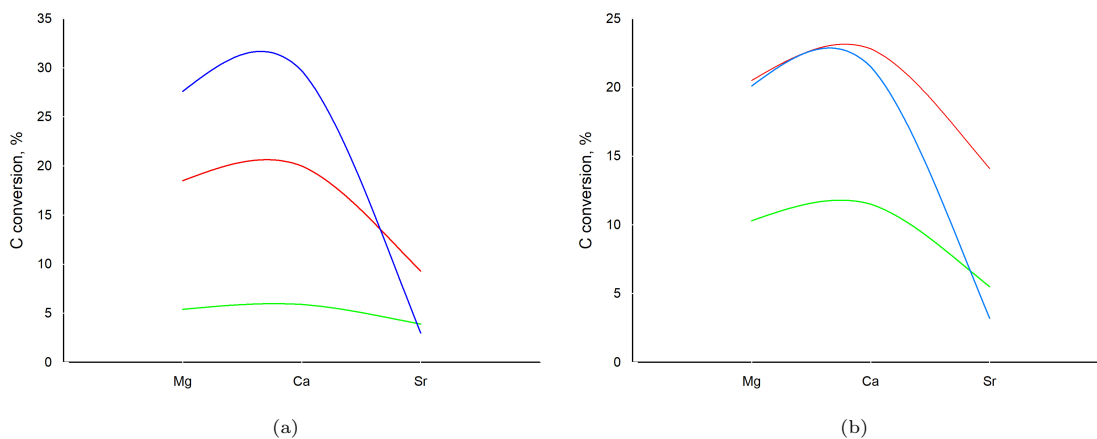


Figure 8: Catalysts maximum carbon conversion at 513 K (a) and 533 K (b) versus basic promoter

244 4. Conclusions

246 Methanol can be produced from biosyngas and streams of CO₂. However, at present, the industrialisation of this process is limited by economic constraints [72]. We doped a typical copper-zinc-alumina catalyst with 1% alkali earth metals to confer the final material basicity. These catalysts 248 synthesize methanol at 2.0 MPa, with co-production of water. Sr resulted inactive towards CO₂ conversion into methanol. With syngas and CO₂/H₂ as feed, CZA-Ca resulted the best catalyst, 250 with a CO conversion of 20% and 6% at 513 K and 24% and 12% at 533 K, respectively. The undoped catalyst possesses the highest CH₃OH selectivity and conversion of CO₂ into methanol, 252 but literature reports low lifetime for these kind of materials. Metal doping tailor catalysts' morphology. Ca and Sr induce the formation of columnar structures. The catalysts were tested for 254 48 h at constant temperature, therefore little information is available on their stability over time, i.e. sintering, poisoning, etc. The synthesis of mixed oxide doped CZA and the effect of different 256 dopants concentration will be the object of future works.

References

- 258 [1] Schellnhuber HJ, Rahmstorf S, Winkelmann R. Why the right climate target was agreed in Paris. *Nature Climate Change* 2016;6(7):649–53. URL: <http://www.nature.com/doi/10.1038/nclimate3013>. doi:10.1038/nclimate3013.
- 260 [2] Al-falahi MD, Jayasinghe S, Enshaei H. A review on recent size optimization methodologies for standalone solar and wind hybrid renewable energy system. *Energy Conversion and Management* 2017;143:252–74. doi:10.1016/j.enconman.2017.04.019.
- 262 [3] Partridge I. Cost comparisons for wind and thermal power generation. *Energy Policy* 2018;112:272–9. doi:10.1016/j.enpol.2017.10.006.
- 264 [4] Global greenhouse gas emissions data. 2020. URL: <https://www.epa.gov/ghgemissions/global-greenhouse-gas-emissions-data>.
- 266 [5] Rahman FA, Aziz MMA, Saidur R, Bakar WAWA, Hainin M, Putrajaya R, et al. Pollution to solution: Capture and sequestration of carbon dioxide (CO₂) and its utilization as a renewable energy source for a sustainable future. *Renewable and Sustainable Energy Reviews* 2017;71:112–26. URL: <http://www.sciencedirect.com/science/article/pii/S136403211730014X>. doi:<https://doi.org/10.1016/j.rser.2017.01.011>.
- 268 [6] Gaede J, Meadowcroft J. Carbon capture and storage demonstration and low-carbon energy transitions: Explaining limited progress. In: de Graaf Thijs V, K. SB, Arunabha G, Florian K, T. KM, editors. *The Palgrave Handbook of the International Political Economy of Energy*. London: Palgrave Macmillan UK. ISBN 978-1-137-55631-8; 2016, p. 319–40. doi:10.1057/978-1-137-55631-8_13.
- 270 [7] Barker R, Hua Y, Neville A. Internal corrosion of carbon steel pipelines for dense-phase CO₂ transport in carbon capture and storage (CCS) – a review. *International Materials Reviews* 2017;62(1):1–31. doi:10.1080/09506608.2016.1176306.
- 272
- 274
- 276
- 278
- 280

- 282 [8] Hasan MMF, Baliban RC, Elia JA, Floudas CA. Modeling, simulation, and optimization
of postcombustion CO₂ capture for variable feed concentration and flow rate. 1. Chem-
284 ical absorption and membrane processes. *Industrial & Engineering Chemistry Research*
2012;51(48):15642–64. doi:10.1021/ie301571d.
- [9] Braun C, Merk C, Pönitzsch G, Rehdanz K, Schmidt U. Public perception of climate en-
286 gineering and carbon capture and storage in germany: survey evidence. *Climate Policy*
2018;18(4):471–84. doi:10.1080/14693062.2017.1304888.
- 288 [10] World energy outlook 2018. 2018. URL: [https://www.iea.org/reports/
world-energy-outlook-2018](https://www.iea.org/reports/world-energy-outlook-2018).
- 290 [11] Centi G, Perathoner S. Opportunities and prospects in the chemical recycling of carbon dioxide
to fuels. *Catalysis Today* 2009;148(3):191 – 205. doi:10.1016/j.cattod.2009.07.075.
- 292 [12] Aresta M, Nocito F. Large scale utilization of carbon dioxide: From its reaction with energy rich
chemicals to (co)-processing with water to afford energy rich products. opportunities and barriers.
294 In: Aresta M, Karimi I, Kawi S, editors. *An Economy Based on Carbon Dioxide and Water*.
Cham: Springer International Publishing; 2019, p. 1–33. doi:10.1007/978-3-030-15868-2_1.
- 296 [13] Tapia JFD, Lee JY, Ooi RE, Foo DC, Tan RR. A review of optimization and decision-making
models for the planning of CO₂ capture, utilization and storage (CCUS) systems. *Sustainable*
298 *Production and Consumption* 2018;13:1 – 15. doi:10.1016/j.spc.2017.10.001.
- [14] Kropp T, Paier J, Sauer J. Oxidative dehydrogenation of methanol at ceria-supported vanadia
300 oligomers. *Journal of Catalysis* 2017;352:382 –7. doi:[https://doi.org/10.1016/j.jcat.
2017.06.011](https://doi.org/10.1016/j.jcat.2017.06.011).
- 302 [15] Gribovskii A, Ovchinnikova E, Vernikovskaya N, Andreev D, Chumachenko V, Makarshin
L. Microchannel reactor for intensifying oxidation of methanol to formaldehyde over Fe-Mo
304 catalyst. *Chemical Engineering Journal* 2017;308:135 –41. doi:[https://doi.org/10.1016/j.
cej.2016.09.058](https://doi.org/10.1016/j.cej.2016.09.058).
- 306 [16] Losch P, Pinar AB, Willinger MG, Soukup K, Chavan S, Vincent B, et al. H-ZSM-5 zeo-
lite model crystals: Structure-diffusion-activity relationship in methanol-to-olefins catalysis.
308 *Journal of Catalysis* 2017;345:11 – 23. doi:<https://doi.org/10.1016/j.jcat.2016.11.005>.
- [17] Wang X, Li R, ul Hasnain Bakhtiar S, Yuan F, Li Z, Zhu Y. Excellent catalytic performance
310 for methanol to olefins over SAPO-34 synthesized by controlling hydrothermal temperature.
Catalysis Communications 2018;108:64 –7. doi:[https://doi.org/10.1016/j.catcom.2018.
312 01.033](https://doi.org/10.1016/j.catcom.2018.01.033).
- [18] Pirola C, Manenti F, Galli F, Bianchi CL, Boffito DC, Corbetta M. Heterogeneously catalyzed
314 free fatty acids esterification in (monophasic liquid)/solid packed bed reactors (PBR). *Chemical*
Engineering Transaction 2014;37:553 –8. doi:<https://doi.org/10.3303/CET1437093>.
- 316 [19] Pirola C, Galli F, Bianchi CL, Boffito DC, Comazzi A, Manenti F. Vegetable oil deacidification
by methanol heterogeneously catalyzed esterification in (monophasic liquid)/solid batch and
318 continuous reactors. *Energy & Fuels* 2014;28(8):5236–40. doi:10.1021/ef501397h.

- 320 [20] Boffito DC, Galli F, Martinez PR, Pirola C, Bianchi C, Patience GS. Transesterification of triglycerides in a new ultrasonic- assisted mixing device. *Chemical Engineering Transaction* 2014;43:427–32. doi:10.3303/CET1543072.
- 322 [21] Niu X, Gao J, Wang K, Miao Q, Dong M, Wang G, et al. Influence of crystal size on the catalytic performance of H-ZSM-5 and zn/H-ZSM-5 in the conversion of methanol to aromatics. *Fuel Processing Technology* 2017;157:99 – 107. doi:https://doi.org/10.1016/j.fuproc.2016.12.006.
- 324 [22] Yang L, Liu Z, Liu Z, Peng W, Liu Y, Liu C. Correlation between H-ZSM-5 crystal size and catalytic performance in the methanol-to-aromatics reaction. *Chinese Journal of Catalysis* 2017;38(4):683–90. doi:https://doi.org/10.1016/S1872-2067(17)62791-8.
- 326 [23] Iaquaniello G, Centi G, Salladini A, Palo E. Methanol economy: Environment, demand, and marketing with a focus on the waste-to-methanol process. In: Basile A, Dalena F, editors. *Methanol*. Elsevier. ISBN 978-0-444-63903-5; 2018, p. 595 – 612. doi:10.1016/B978-0-444-63903-5.00022-4.
- 330 [24] Alvarado M. The changing face of the global methanol industry. *IHS Chemical Bulletin* 2016;3(6083):10–1.
- 332 [25] Behrens M, Studt F, Kasatkin I, Kühl S, Hävecker M, Abild-Pedersen F, et al. The active site of methanol synthesis over Cu/ZnO/Al₂O₃ industrial catalysts. *Science* 2012;336(6083):893–7. doi:10.1126/science.1219831.
- 334 [26] Robinson W, Mol J. Copper surface area and activity in CO/H₂ of Cu/ZnO/Al₂O₃ methanol synthesis catalysts. *Applied Catalysis* 1990;60(1):73 – 86. doi:10.1016/S0166-9834(00)82173-9.
- 336 [27] Azizi Z, Rezaeimanesh M, Tohidian T, Rahimpour MR. Dimethyl ether: A review of technologies and production challenges. *Chemical Engineering and Processing: Process Intensification* 2014;82:150–72. doi:10.1016/j.cep.2014.06.007.
- 338 [28] Doesburg E, Höppener R, de Koning B, Xiaoding X, Scholten J. Preparation and characterization of copper/zinc oxide/alumina catalysts for methanol synthesis. In: Delmon B, Grange P, Jacobs P, Poncelet G, editors. *Preparation of Catalysts IV*; vol. 31 of *Studies in Surface Science and Catalysis*. Elsevier; 1987, p. 767–83. doi:10.1016/S0167-2991(08)65452-X.
- 340 [29] Fitzpatrick T, Hicks T. Catalysts with higher and more stable activity enable cost saving and boost output in methanol production. *Catalysis* 2010;15:47 – 53. URL: https://www.digitalrefining.com/data/digital_magazines/file/1717768075.pdf.
- 342 [30] Lunkenbein T, Girgsdies F, Kandemir T, Thomas N, Behrens M, Schlögl R, et al. Bridging the time gap: A copper/zinc oxide/aluminum oxide catalyst for methanol synthesis studied under industrially relevant conditions and time scales. *Angewandte Chemie International Edition* 2016;55(41):12708–12. doi:10.1002/anie.201603368.
- 344 [31] English A, Rovner J, Brown J, Davies Sa. Methanol. In: *Kirk-Othmer Encyclopedia of Chemical Technology*; chap. 16. American Cancer Society. ISBN 9780471238966; 2005, p. 299–316. doi:10.1002/0471238961.1305200805140712.a01.pub2.

- 358 [32] Yang L, Ge X. Chapter three - biogas and syngas upgrading. vol. 1 of *Advances in Bioenergy*. Elsevier; 2016, p. 125–88. doi:10.1016/bs.aibe.2016.09.003.
- 360 [33] Ertl G, Knözinger H, Weitkamp J. Handbook of heterogeneous catalysis. Wiley; 2008. doi:10.1002/9783527619474.
- 362 [34] Clausen LR, Houbak N, Elmegaard B. Technoeconomic analysis of a methanol plant based on gasification of biomass and electrolysis of water. *Energy* 2010;35(5):2338–47. doi:10.1016/j.energy.2010.02.034.
- 364 [35] Meshkini F, Taghizadeh M, Bahmani M. Investigating the effect of metal oxide additives on the properties of Cu/ZnO/Al₂O₃ catalysts in methanol synthesis from syngas using factorial experimental design. *Fuel* 2010;89(1):170–5. doi:10.1016/j.fuel.2009.07.007.
- 366 [36] Baltes C, Vukojevic S, Schuth F. Correlations between synthesis, precursor, and catalyst structure and activity of a large set of CuO/ZnO/Al₂O₃ catalysts for methanol synthesis. *Journal of Catalysis* 2008;258(2):334–44. doi:10.1016/j.jcat.2008.07.004.
- 368 [37] Wang Y, Kattel S, Gao W, Li K, Liu P, Chen JG, et al. Exploring the ternary interactions in Cu–ZnO–ZrO₂ catalysts for efficient CO₂ hydrogenation to methanol. *Nature communication* 2019;10:1–10. doi:10.1038/s41467-019-09072-6.
- 370 [38] Brunauer S, Emmett PH, Teller E. Adsorption of gases in multimolecular layers. *Journal of the American Chemical Society* 1938;60(2):309–19. doi:10.1021/ja01269a023.
- 372 [39] Barrett EP, Joyner LG, Halenda PP. The determination of pore volume and area distributions in porous substances. i. Computations from nitrogen isotherms. *Journal of the American Chemical Society* 1951;73(1):373–80. doi:10.1021/ja01145a126.
- 374 [40] Pirola C, Galli F, Patience GS. Experimental methods in chemical engineering: Temperature programmed reduction—TPR. *The Canadian Journal of Chemical Engineering* 2018;96(11):2317–20. doi:10.1002/cjce.23317.
- 376 [41] Skoog DA, West DM, Holler FJ, Crouch SR. Fundamentals of analytical chemistry. Nelson Education; 2013.
- 378 [42] Lutz AE, Bradshaw RW, Keller JO, Witmer DE. Thermodynamic analysis of hydrogen production by steam reforming. *International Journal of Hydrogen Energy* 2003;28(2):159–67. doi:10.1016/S0360-3199(02)00053-8.
- 380 [43] Wei J, Iglesia E. Isotopic and kinetic assessment of the mechanism of reactions of CH₄ with CO₂ or H₂O to form synthesis gas and carbon on nickel catalysts. *Journal of Catalysis* 2004;224(2):370–83. doi:10.1016/j.jcat.2004.02.032.
- 382 [44] Comazzi A, Pirola C, Bianchi CL, Galli F, Longhi M, Manenti F. High-loaded Fe-supported catalyst for the thermochemical BtL-FT process: Experimental results and modelling. *The Canadian Journal of Chemical Engineering* 2016;94(4):696–702. doi:10.1002/cjce.22357.
- 384 [45] Comazzi A, Pirola C, Michele AD, Compagnoni M, Galli F, Rossetti I, et al. Flame spray pyrolysis as fine preparation technique for stable CO and CO/RU based catalysts for FT process. *Applied Catalysis A: General* 2016;520:92–8. doi:10.1016/j.apcata.2016.04.010.
- 386

- 396 [46] Louyot P, Neagoe C, Galli F, Pirola C, Patience GS, Boffito DC. Ultrasound-assisted impreg-
398 nation for high temperature Fischer-Tropsch catalysts. *Ultrasonics Sonochemistry* 2018;48:523
–31. doi:10.1016/j.ultsonch.2018.06.017.
- [47] Panigrahi S, Dalai AK, Chaudhari ST, Bakhshi NN. Synthesis gas production from steam
400 gasification of biomass-derived oil. *Energy & Fuels* 2003;17(3):637–42. doi:10.1021/ef020073z.
- [48] Bozzano G, Manenti F. Efficient methanol synthesis: Perspectives, technologies and optimiza-
402 tion strategies. *Progress in Energy and Combustion Science* 2016;56:71 – 105. doi:10.1016/
j.peccs.2016.06.001.
- [49] Saeidi S, Amin NAS, Rahimpour MR. Hydrogenation of CO₂ to value-added products—a
404 review and potential future developments. *Journal of CO2 Utilization* 2014;5:66 – 81. doi:10.
406 1016/j.jcou.2013.12.005.
- [50] Ginés MJL, Apesteguía CR. Thermal decomposition of cu-based hydroxycarbonate cat-
408 alytic precursors for the low-temperature co-shift reaction. *Journal of thermal analysis*
1997;50(5):745–56. doi:10.1007/BF01979204.
- [51] Zhang F, Zhang Y, Yuan L, Gasem KA, Chen J, Chiang F, et al. Synthesis of Cu/Zn/Al/Mg
410 catalysts on methanol production by different precipitation methods. *Journal of Molecular*
412 *Catalysis* 2017;441:190–8. doi:10.1016/j.mcat.2017.08.015.
- [52] Frost R, Ding Z, Klopogge J, Martens W. Thermal stability of azurite and malachite in
414 relation to the formation of mediaeval glass and glazes. *Thermochimica Acta* 2002;390(1):133
–44. doi:10.1016/S0040-6031(02)00127-2.
- [53] Kanari N, Mishra D, Gaballah I, Dupré B. Thermal decomposition of zinc carbonate hydroxide.
416 *Thermochimica Acta* 2004;410(1):93 – 100. doi:10.1016/S0040-6031(03)00396-4.
- [54] Zander S, Kunkes EL, Schuster ME, Schumann J, Weinberg G, Teschner D, et al. The role
418 of the oxide component in the development of copper composite catalysts for methanol syn-
thesis. *Angewandte Chemie International Edition* 2013;52(25):6536–40. doi:10.1002/anie.
420 201301419.
- [55] Verrecchia EP, Verrecchia KE. Needle-fiber calcite; a critical review and a pro-
422 posed classification. *Journal of Sedimentary Research* 1994;64(3a):650–64. doi:10.1306/
424 D4267E33-2B26-11D7-8648000102C1865D.
- [56] Haynes W. *CRC Handbook of Chemistry and Physics*, 93rd Edition. Taylor & Francis; 2012.
426 ISBN 9781439880494.
- [57] Gamsjager H, Konigsberger E, Preis W. Solubilities of metal carbonates. *Pure and Applied*
428 *Chemistry* 2019;70:1913 –20. doi:10.1351/pac199870101913.
- [58] Li JL, Inui T. Characterization of precursors of methanol synthesis catalysts, cop-
430 per/zinc/aluminum oxides, precipitated at different pHs and temperatures. *Applied Catalysis*
A: General 1996;137(1):105 –17. doi:10.1016/0926-860X(95)00284-7.
- [59] Lenormand J, Salman T, Yoon RH. Hydroxamate flotation of malachite. *Canadian Metallur-*
432 *gical Quarterly* 1979;18(2):125–9. doi:10.1179/cmq.1979.18.2.125.

- 434 [60] Reddy S, Rautaray D, Sainkar SR, Sastry M. On the morphology of SrCO₃ crystals grown
436 at the interface between two immiscible liquids. *Bulletin of Materials Science* 2003;26(3):283.
doi:10.1007/BF02707447.
- [61] Agrawal SG, Paterson AHJ. Secondary nucleation: Mechanisms and models. *Chemical Engi-
438 neering Communications* 2015;202(5):698–706. doi:10.1080/00986445.2014.969369.
- [62] Lee WJ, Bordoloi A, Patel J, Bhatelia T. The effect of metal additives in Cu/Zn/Al₂O₃ as a
440 catalyst for low-pressure methanol synthesis in an oil-cooled annulus reactor. *Catalysis Today*
2019;doi:10.1016/j.cattod.2019.03.041.
- [63] Chu Z, Chen H, Yu Y, Wang Q, Fang D. Surfactant-assisted preparation of Cu/ZnO/Al₂O₃
442 catalyst for methanol synthesis from syngas. *Journal of Molecular Catalysis A: Chemical*
444 2013;366:48 – 53. doi:10.1016/j.molcata.2012.09.007.
- [64] García-Trenco A, Martínez A. A rational strategy for preparing Cu-ZnO/H-ZSM-5 hybrid
446 catalysts with enhanced stability during the one-step conversion of syngas to dimethyl ether
(DME). *Applied Catalysis A: General* 2015;493:40 –9. doi:10.1016/j.apcata.2015.01.007.
- [65] jing Lu P, feng Cai F, Zhang J, yu Liu Y, han Sun Y. Hydrogen production from methanol
448 steam reforming over B-modified CuZnAlO_x catalysts. *Journal of Fuel Chemistry and Tech-
450 nology* 2019;47(7):791 –8. doi:10.1016/S1872-5813(19)30035-0.
- [66] Wang L, Yang L, Zhang Y, Ding W, Chen S, Fang W, et al. Promoting effect of an aluminum
452 emulsion on catalytic performance of Cu-based catalysts for methanol synthesis from syngas.
Fuel Processing Technology 2010;91(7):723 –8. doi:10.1016/j.fuproc.2010.02.003.
- [67] Lefebvre J, Galli F, Bianchi CL, Patience GS, Boffito DC. Experimental methods in chemi-
454 cal engineering: X-ray photoelectron spectroscopy-xps. *The Canadian Journal of Chemical*
456 *Engineering* 2019;0(ja). doi:10.1002/cjce.23530.
- [68] Behrens M, Brennecke D, Girgsdies F, Kißner S, Trunschke A, Nasrudin N, et al. Understanding
458 the complexity of a catalyst synthesis: Co-precipitation of mixed Cu, Zn, Al hydroxycarbon-
ate precursors for Cu/ZnO/Al₂O₃ catalysts investigated by titration experiments. *Applied*
460 *Catalysis A: General* 2011;392(1):93 – 102. doi:10.1016/j.apcata.2010.10.031.
- [69] Liu C, Guo X, Guo Q, Mao D, Yu J, Lu G. Methanol synthesis from CO₂ hydrogenation
462 over copper catalysts supported on MgO-modified TiO₂. *Journal of Molecular Catalysis A:
Chemical* 2016;425:86 – 93. doi:10.1016/j.molcata.2016.09.032.
- [70] Phongamwong T, Chantaprasertporn U, Witoon T, Numpilai T, Poo-arporn Y, Limphirat W,
464 et al. CO₂ hydrogenation to methanol over CuO–ZnO–ZrO₂–SiO₂ catalysts: Effects of SiO₂
466 contents. *Chemical Engineering Journal* 2017;316:692 – 703. doi:10.1016/j.cej.2017.02.010.
- [71] Li L, Mao D, Yu J, Guo X. Highly selective hydrogenation of CO₂ to methanol over
468 CuO–ZnO–ZrO₂ catalysts prepared by a surfactant-assisted co-precipitation method. *Jour-
nal of Power Sources* 2015;279:394 – 404. doi:10.1016/j.jpowsour.2014.12.142.
- [72] Meunier N, Chauvy R, Mouhoubi S, Thomas D, Weireld] GD. Alternative production of
470 methanol from industrial CO₂. *Renewable Energy* 2020;146:1192 –203. doi:10.1016/j.
472 *renene*.2019.07.010.